IEEE Access
Multidisciplinary | Rapid Review | Open Access Journal

Received January 29, 2021, accepted February 9, 2021, date of publication February 12, 2021, date of current version February 23, 2021.

Digital Object Identifier 10.1109/ACCESS.2021.3059157

Direction-of-Arrival Estimation of Far-Field Sources Under Near-Field Interferences in Passive Sonar Array

HOJUN LEE, JONGMIN AHN, YONGCHEOL KIM, AND JAEHAK CHUNG
Department of Electronics Engineering, Inha University, Incheon 22212, South Korea

Corresponding author: Jaehak Chung (jchung@inha.ac.kr)

This work was supported by the Inha University Research Program.

ABSTRACT For passive sonar arrays, when far-field sources lie in a masking region caused by near-field interferences, direction-of-arrival (DOA) estimations of the interfered far-field sources become difficult. To mitigate the interference, we propose a near-field interference mitigation (NFIM) beamformer that utilizes subarrays and a proposed azimuth-domain filter without any source constraint. For the proposed method, this paper mathematically analyzes the masking region and the subarray configuration to separate the beams of the far-field source from the near-field interference and designs the proposed azimuth-domain filter in the proposed zeta domain. The suppression filter is implemented for all subarrays to mitigate the interferences, and the filtered outputs of all subarrays are combined to suppress residual interferences. Computer simulations show that the proposed NFIM beamformer mitigates the interferences and increases the DOA estimation performance compared with those of conventional methods.

INDEX TERMS Direction-of-arrival estimation, interference suppression, array signal processing, sonar detection.

ABBREVIATION

BTR	Bearing time record
DAS	Delay-and-sum
DOA	Direction-of-arrival
INR	Interference-to-noise power ratio
MF	Matrix filter
MFN	Matrix filter with nulling
MVDR	Minimum variance distortionless response
NFFF	Near-field/far-field
NFIM	Near-field interference mitigation
PAPR	Peak-to-average power ratio
SIR	Signal-to-interference power ratio
SNR	Signal-to-noise power ratio
RMSE	Root mean square error
ULA	Uniform line array

I. INTRODUCTION

Passive sonar arrays have been utilized for estimating the distances and the direction-of-arrivals (DOAs) of various sources [1]–[4]. The delay-and-sum (DAS) beamforming method has been widely used for estimating the DOAs of far-field sources. In the DAS method, if vessels and ships are closely located to the sonar array, their received powers at sonar sensors are larger than those from the far-field source. In addition, the phase mismatches by the DAS cause a masking region with a large and wide beam in the azimuth domain [5], [6]. When the DOA of the far-field source lies in the masking region, the DOA estimation of the far-field sources becomes difficult to achieve with near-field interferers [7]–[11].

Interference mitigation techniques in sonar arrays have been researched to solve masking problems [11], [12]. In [11], a near-field/far-field (NFFF) beamformer, which is based on a minimum variance distortionless response (MVDR), was studied to remove near-field interference by the weight vector of the beamformer. The NFFF beamformer, however, required the same center frequencies of the far-field sources, which is impractical. In [12], the main-beam and null patterns of a sonar array were designed to null the interference, but two sources had to be located in the far-field region with different azimuths. In [13], [14], researchers designed a matrix filter (MF) that suppressed the near-field beam power. However, when the DOAs of the far- and near-field sources

The associate editor coordinating the review of this manuscript and approving it for publication was Chengpeng Hao.

were similar, the DOA estimation performance was degraded. In [15], [16], a matrix filter with nulling (MFN) was studied. Even if the MFN suppressed the near-field beam powers, the masking regions persisted.

This paper proposes a near-field interference mitigation (NFIM) beamformer that improves the DOA estimation performance of the interfered far-field source for a uniform line array (ULA) without any source constraint. The proposed method separates the beams of the far-field source from those of the near-field interference by using the subarrays in the azimuth domain and suppresses the interferences using an azimuth-domain filter. For designing both the subarray and the azimuth-domain filter, the masking region is mathematically analyzed in the azimuth and proposed zeta domains, and a subarray configuration for beam separation is derived. The azimuth-domain filter suppressing the near-field interferers is developed based on the difference between the beamwidths of the near-field and far-field sources in the azimuth domain. The designed suppression filter is applied to all subarrays, and all filtered outputs are averaged to remove residual interferences. Computer simulations demonstrate that the proposed NFIM beamformer reduces the interference and improves the DOA estimation performance.

The contributions of this paper are threefold:

- We mathematically derive the masking region for the ULA in the azimuth domain.
- We mathematically analyze the subarray configuration of the beam separation even if the DOAs of the far- and near-field sources are similar.
- We propose an azimuth-domain filter to suppress the near-field beam power and the zeta domain to design the filter.

This paper consists of six sections. Section 2 analyzes the masking region. Section 3 derives the subarray configuration for separating the beams of the far-field source from the near-field interference. Section 4 describes the proposed NFIM beamformer. In section 5, computer simulations are executed to show that the DOA estimation performance of the proposed beamformer is better than those of the conventional methods. Section 6 concludes the paper.

II. MASKING REGION ANALYSIS

The masking region for the ULA is analyzed in the azimuth domain. Assume that the passive sonar array has N sensors with l sensor distance; one far-field source is located at an azimuth (θ_F), and one near-field interferer is at a distance (d_N) with an azimuth (θ_N). Let f_F and f_N be the center frequencies of the far- and near-field signals, respectively. Then, the received signal of the j-th sensor ($r_j(t)$) can be expressed as

$$r_j(t) = exp\left\{-j2\pi f_F \tau_j(\theta_F)\right\} s_F(t) + exp\left\{-j2\pi f_N \tilde{\tau}_j(d_N, \theta_N)\right\} s_N(t) + n_j(t), \quad (1)$$

where $s_F(t)$, $s_N(t)$, and $n_j(t)$ denote the far- and near-field signals and the received noise of the j-th sensor, respectively.

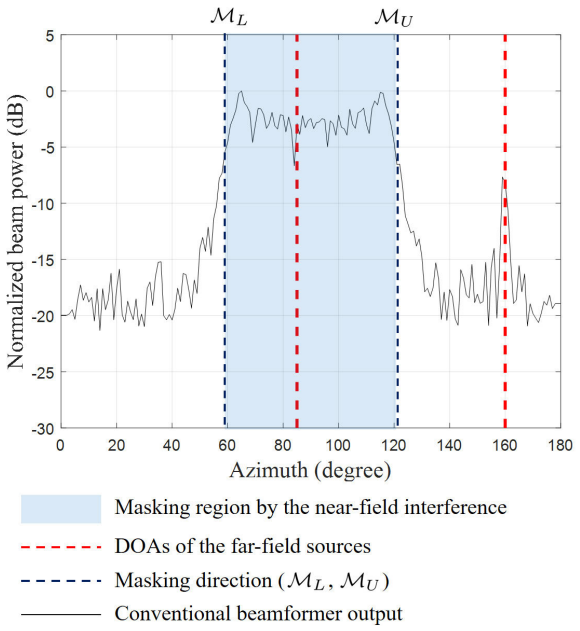

FIGURE 1. Masking region by the near-field interference in the azimuth domain.

$\tau_j(\theta_F)$ and $\tilde{\tau}_j(d_N, \theta_N)$ denote the relative propagation delays of the j-th sensor with respect to the first sensor of the far- and near-field signals, respectively. The wavefronts of the far- and near-field signals at the sonar sensors have plane and spherical waves, respectively. Let the first sensor be a reference element and c denote the sound speed underwater. Then, $\tau_j(\theta_F)$ and $\tilde{\tau}_j(d_N, \theta_N)$ are represented as

$$\tau_j(\theta_F) = l(j-1)\sin\theta_F / c, \quad (2)$$

$$\tilde{\tau}_j(d_N, \theta_N) = \frac{1}{c}\sqrt{\left\{d_N\cos\theta_N + \frac{(N-2j+1)}{2}l\right\}^2 + d_N^2\sin^2\theta_N} - \frac{1}{c}\sqrt{\left\{d_N\cos\theta_N + \frac{(N-1)}{2}l\right\}^2 + d_N^2\sin^2\theta_N}. \quad (3)$$

In general, the conventional DAS beamformer is designed for the far-field signal and calculates the propagation delays at all sensors by using (2). When the conventional DAS beamformer detects near-field interference, phase mismatches between (2) and (3) occur, and the main beam of the near-field interference forms a wide masking region with large power, as shown in Fig. 1. In Fig. 1, the masking region by the near-field interference is formed from the lower masking direction ($\mathcal{M}_L$) to the upper masking direction ($\mathcal{M}_U$), and the far-field source located in the masking region is undetectable. Thus, this paper analyzes the masking region to develop both the subarray configuration and the azimuth-domain filter that improve the DOA estimation performance of the interfered far-field sources.

The geometrical masking region of the sonar array is depicted in Fig. 2. In Fig. 2, the largest phase mismatches occur at both end-fire sensors of the array, and the masking

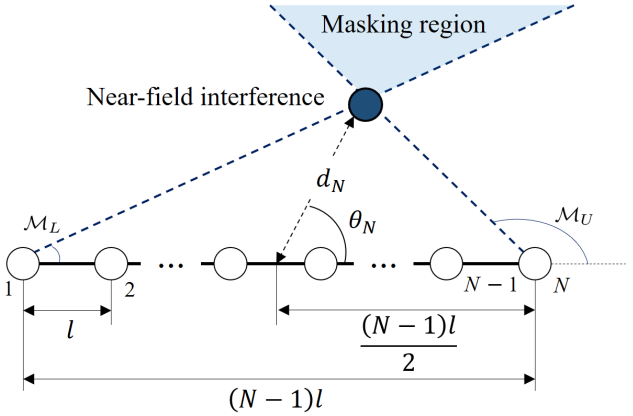

FIGURE 2. Geometrical structure of the masking region.

region can be geometrically determined by the angles between the two end-fire sensors and the near-field interference location. Let the angles of the near-field interference and the left- and right-end sensors be the lower masking direction ($\mathcal{M}_L$) and the upper masking direction ($\mathcal{M}_U$), respectively, in Fig. 2. $\mathcal{M}_L$ and $\mathcal{M}_U$ are calculated as

$$\mathcal{M}_L(N, l, d_N, \theta_N) = \begin{cases} \theta_N - \arctan\left\{\dfrac{(N-1)\,l}{2d_N}\right\}, & \text{if } \theta_N = \dfrac{\pi}{2} \\ \dfrac{\pi}{2} - \arctan\left\{\dfrac{(N-1)\,l/2 + d_N\cos\theta_N}{d_N\sin\theta}\right\}, & \text{otherwise} \end{cases} \tag{4}$$

$$\mathcal{M}_U(N, l, d_N, \theta_N) = \begin{cases} \theta_N + \arctan\left\{\dfrac{(N-1)\,l}{2d_N}\right\}, \\ \qquad \text{if } \theta_N = \dfrac{\pi}{2} \\ \pi - \arctan\left\{\dfrac{d_N\sin\theta}{(N-1)\,l/2 - d_N\cos\theta_N}\right\}, \\ \qquad \text{else if } \frac{(N-1)l}{2} \geq d_N\cos\theta_N \\ -\arctan\left\{\dfrac{d_N\sin\theta_N}{(N-1)\,l/2 - d_N\cos\theta_N}\right\}, \\ \qquad \text{otherwise} \end{cases} \tag{5}$$

For the full array in Fig. 1, when the far-field sources with the small beam powers are located in the masking region with the strong beam power, the main beams of the far-field sources are masked by the near-field interference. Thus, the full array cannot detect the far-field sources in the masking region. However, if the subarrays that consist of partial sections of the full array are utilized, the masking regions vary by the subarrays as shown in Fig. 3, but the DOA of the far-field sources in all subarrays are the same. Therefore, if the subarray is properly configured, the beams of the far-field sources are located out of the masking region and can be detected. In the next section, the subarray configuration for the beam separation of the far-field source from the near-field interference is analyzed.

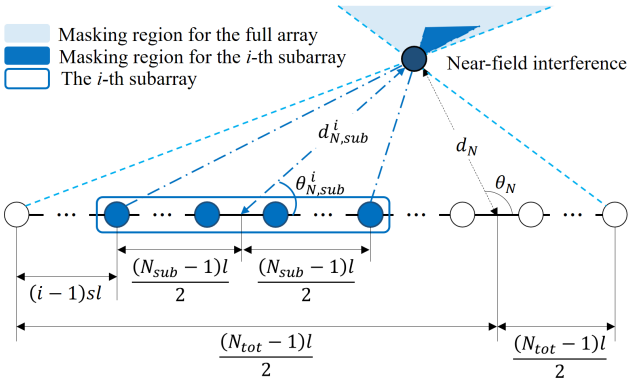

FIGURE 3. Geometrical structures of the masking regions for the full array and the *i*-th subarray.

III. SUB-ARRAY ANALYSIS

Assume that the number of sensors of the full array and the subarray are N_{tot} and N_{sub}, respectively, the sensor distance is l, the stride separating the subarrays is s, and the set of integer numbers is $\mathbb{Z}$. Then, the number of configurable subarrays (N_{vol}) is obtained by $\max\{n \in \mathbb{Z} \mid n \leq (N_{tot} - N_{sub})/s + 1\}$, and an example of the i-th subarray is shown in Fig. 3.

In Fig. 3, the near-field interference is located at a distance ($d^i_{N,sub}$) and an azimuth ($\theta^i_{N,sub}$) from the i-th subarray, which are calculated as

$$d^i_{N,sub} = \sqrt{{d_N}^2\sin^2\theta_N + (d_N\cos\theta_N + C_i)^2}, \tag{6}$$

$$\theta^i_{N,sub} = \begin{cases} \arctan\left\{\dfrac{d_N\sin\theta_N}{d_N\cos\theta_N + C_i}\right\}, \\ \qquad \text{if } d_N\cos\theta_N + C_i > 0 \\ \pi + \arctan\left\{\dfrac{d_N\sin\theta_N}{d_N\cos\theta_N + C_i}\right\}, \\ \qquad \text{otherwise} \end{cases} \tag{7}$$

where

$$C_i = (N_{tot} - N_{sub})\,l/2 - (i-1)\,sl. \tag{8}$$

The masking region for the i-th subarray is obtained by substituting (6) and (7) into (4) and (5). The lower and upper masking directions of the i-th subarray, i.e., $\mathcal{M}^i_{L,sub}$ and $\mathcal{M}^i_{U,sub}$, respectively, are expressed as

$$\mathcal{M}^i_{L,sub} = \mathcal{M}_L\left(N_{sub}, l, d^i_{N,sub}, \theta^i_{N,sub}\right), \tag{9}$$

$$\mathcal{M}^i_{U,sub} = \mathcal{M}_U\left(N_{sub}, l, d^i_{N,sub}, \theta^i_{N,sub}\right). \tag{10}$$

Even if the near-field interference and the far-field source have the same DOA for the full array, i.e., $\theta_N = \theta_F$, the subarray can separate the beams of the far-field source from those of the near-field interference. The beam separation of two sources by the subarray occurs when θ_F is greater than the upper masking direction of the first or last subarrays or θ_F is

smaller than the lower masking direction of the first or last subarrays. These requirements are given as

$$\theta_N = \theta_F > \mathcal{M}^{1}_{U,sub}, \tag{11}$$
$$\theta_N = \theta_F > \mathcal{M}^{N_{vol}}_{U,sub}, \tag{12}$$
$$\theta_N = \theta_F < \mathcal{M}^{1}_{L,sub}, \tag{13}$$
$$\theta_N = \theta_F < \mathcal{M}^{N_{vol}}_{L,sub}. \tag{14}$$

For a simple calculation, assuming $\theta_F = \theta_N = \pi/2$, which is the worst case to separate the beams of two sources, the masking region becomes symmetric, and (11) is the same as (12)-(14). From (6), (7) and (10), $\mathcal{M}^{1}_{U,sub}$ is represented as

$$\mathcal{M}^{1}_{U,sub} = \begin{cases} \pi - \arctan\left\{\dfrac{d_N}{(N_{sub}-1)\,l/2-(N_{tot}-N_{sub})\,l/2}\right\}, \\ \quad \text{for } (N_{sub}-1)\,l/2 \geq (N_{tot}-N_{sub})\,l/2 \\ -\arctan\left\{\dfrac{d_N}{(N_{sub}-1)\,l/2-(N_{tot}-N_{sub})\,l/2}\right\}, \\ \quad \text{for } (N_{sub}-1)\,l/2 < (N_{tot}-N_{sub})\,l/2 \end{cases} \tag{15}$$

Equation (10) is combined with (15) and is rewritten as

$$\begin{cases} \arctan\left\{\dfrac{d_N}{(N_{sub}-1)\,l/2-(N_{tot}-N_{sub})\,l/2}\right\} > \dfrac{\pi}{2}, \\ \quad \text{for } (N_{sub}-1)\,l/2 \geq (N_{tot}-N_{sub})\,l/2 \\ \arctan\left\{\dfrac{d_N}{(N_{sub}-1)\,l/2-(N_{tot}-N_{sub})\,l/2}\right\} > -\dfrac{\pi}{2}, \\ \quad \text{for } (N_{sub}-1)\,l/2 < (N_{tot}-N_{sub})\,l/2 \end{cases} \tag{16}$$

The function of an arctan has a value from $-\pi/2$ to $\pi/2$ exclusive. If $(N_{sub}-1)\,l/2 \geq (N_{tot}-N_{sub})\,l/2$, (16) is mathematically contradictory. However, when $(N_{sub}-1)\,l/2 < (N_{tot}-N_{sub})\,l/2$, (16) is always satisfied. Therefore, for $\theta_F = \theta_N$, the beam separation of the far-field source from the near-field interference occurs at $(N_{sub}-1)\,l/2 < (N_{tot}-N_{sub})\,l/2$, which is briefly rewritten as

$$N_{sub} < \frac{N_{tot}+1}{2}. \tag{17}$$

In (17), to detect the DOA of the interfered far-field source using the subarray, the number of subarrays (N_{sub}) is less than or equal to half of N_{tot} sensors because N_{sub} and N_{tot} are natural numbers.

IV. PROPOSED BEAMFORMER

The subarray approach can separate the beams of the far-field signal from the near-field signal for most cases, but not all. Even if the subarray succeeds in separating the far-field source from the masking region, the detection of the far-field source is still difficult since the near-field beam power is relatively strong. Thus, mitigation of the near-field interferences is needed.

In this paper, we develop a filter that removes the interferences from the subarray DAS outputs, i.e., the azimuth domain. The concept of the interference rejection filter is based on the different azimuth beamwidths between the near-field interferers and the far-field sources. As in section 2, the beamwidths of the near-field and far-field sources are wide and narrow, respectively. If the wide beams are filtered out, the narrow beams remain and are detectable.

Since a key factor of the filter is to suppress the wide beams of the near-field sources in the DAS output, we develop a discrimination parameter based on the beamwidth in the azimuth domain. If the total azimuth angle (π) normalizes the beamwidth, the relative beamwidths are obtained. If the relative beamwidth is transformed into a novel domain that consists of a parameter (ζ) with an inverse of the relative width, all beams in the azimuth domain can be expressed in the new zeta domain. This is similar to the fact that rectangular pulses with different widths in the time domain are expressed in different frequencies in the frequency domain by the Fourier transform. Then, using the zeta transform, a wider beamwidth in the azimuth domain is transformed to a smaller value of ζ, and vice versa. Thus, if a filter that passes larger values than the threshold of a ζ value is designed and is applied to the subarray outputs, the near-field interferences are suppressed. In this section, we mathematically develop the proposed NFIM beamformer.

Assume that the received signal of the j-th sensor is $r_j(t)$, and the number of near-field interferences is K. The conventional DAS output ($b^{i}_{sub}(\theta,t)$) at an arbitrary azimuth (θ) of the i-th subarray is given as

$$b^{i}_{sub}(\theta,t) = \sqrt{\frac{1}{T}\int_{t}^{t+T}\left|\sum_{j=1+(i-1)s}^{N_{sub}+(i-1)s} r_j\left(\tilde{t}+\tau_{j,\theta}\right)\right|^2 d\tilde{t}}, \tag{18}$$

where T denotes the time duration for a time average of the received signal.

The masking region caused by the k-th near-field interference of the i-th subarray is given from $\mathcal{M}^{i,k}_{L,sub}$ to $\mathcal{M}^{i,k}_{U,sub}$ in the azimuth domain by (9) and (10). Since the masking region in the azimuth domain is considered the beamwidth of the near-field interference, the beamwidth of the k-th near-field interference is calculated by $\theta^{i,k}_{\mathcal{M}} (= \mathcal{M}^{i,k}_{U,sub} - \mathcal{M}^{i,k}_{L,sub})$. A zeta-domain parameter ($\zeta^{i,k}_{\mathcal{M}}$) corresponding to $\theta^{i,k}_{\mathcal{M}}$ in the azimuth domain is attained as

$$\zeta^{i,k}_{\mathcal{M}} = \frac{\pi}{\theta^{i,k}_{\mathcal{M}}}. \tag{19}$$

The zeta components of the i-th subarray beamformer output ($B^{i}_{sub}(\zeta,t)$) are expressed as

$$B^{i}_{sub}(\zeta,t) = \int_{-\pi/2}^{\pi/2} b^{i}_{sub}(\theta,t)\, e^{j2\pi\zeta\theta} d\theta, \tag{20}$$

where the zeta component of the k-th near-field interference is found at $|\zeta| = \zeta^{i,k}_{\mathcal{M}}$. Thus, if the zeta component

at $|\zeta| = \zeta_{\mathcal{M}}^{i,k}$ in (20) is filtered out, the k-th near-field interference can be removed.

For the multiple interferences, assume that the k^*-th interference is the smallest beamwidth among the interferences, i.e., $k^* = \arg\max_k \zeta_{\mathcal{M}}^{i,k}$. If the filter is designed to filter zeta values less than $|\zeta| < \zeta_{\mathcal{M}}^{i,k^*}$, all wider beams of the interferences are removed. Thus, the filter requirement ($W^{\,i}(\zeta)$) in the zeta domain is given as

$$W^{\,i}(\zeta) = \begin{cases} 0, & \text{for } |\zeta| < \zeta_{\mathcal{M}}^{i,k^*} \\ 1, & \text{otherwise} \end{cases} \tag{21}$$

The suppression filter ($A^{\,i}(\theta)$) in the azimuth domain can be obtained as

$$A^{\,i}(\theta) = \frac{1}{\pi} \int_{-\pi/2}^{\pi/2} W^{\,i}(\zeta) e^{-j2\pi\zeta\theta} d\zeta. \tag{22}$$

Equation (22) denotes the transform from the zeta domain to the azimuth domain for ($W^{\,i}(\zeta)$) as in (20).

When the suppression filter is executed for the outputs of the subarrays, the designed filter may be unable to remove the near-field interferences since the power difference between near-field and far-field sources is very large. To increase the filter performance, the small values in the azimuth domain need to increase, and the large values need to decrease. Thus, a nonlinear function ($f(\cdot)$), e.g., a log function, is utilized for the beam powers of the i-th subarray, which is $\tilde{b}_{sub}^{\,i}(\theta, t)$. The suppression filter ($A^{\,i}(\theta)$) is applied to the nonlinear transform outputs of all subarrays.

The normal output of the suppressed interferences for the i-th subarray ($b_M^i(\theta)$) is attained by applying to the inverse of the nonlinear function, which is expressed as

$$b_M^i(\theta, t) = f^{\,-1}[\tilde{b}_{sub}^{\,i}(\theta, t) * A^{\,i}(\theta)], \tag{23}$$

where $*$ denotes a convolution operator.

In (23), the filtered subarray DAS outputs $b_M^i(\theta, t)$ may have residual interferences. The azimuths and beamwidths of the interferences of all subarrays are different, whereas those of the far-field sources are the same. Thus, if all filtered outputs by (23) are summed, the residual interferences are mitigated, and the beam powers of the far-field sources increase. The proposed NFIM beamformer output ($b_{prop}(\theta, t)$) with the N_{vol} subarrays is calculated as

$$b_{prop}(\theta, t) = \sum_{i=1}^{N_{vol}} b_M^i(\theta, t). \tag{24}$$

Therefore, the proposed NFIM beamformer increases the DOA estimation performance of the interfered far-field source by suppressing the interference and by combining all filtered results.

Let the number of beams be N_{beam}. The proposed NFIM beamformer executes the convolution N_{vol} times on all subarray beamformer outputs. The computational complexities of the proposed NFIM beamformer and the conventional NFFF in [11] are shown in Table 1. Since N_{tot} is always greater than N_{vol} and less than N_{beam}, the proposed beamformer has lower computational complexity than that of the conventional NFFF.

TABLE 1. Comparison of the complexity.

Scheme	Proposed	NFFF
Complexity	$O\left(N_{vol}N_{beam}^2\right)$	$\begin{cases} O\left(N_{tot}^3\right), & \text{for } N_{tot} < N_{beam} \\ O\left(N_{tot}N_{beam}^2\right), & \text{otherwise} \end{cases}$

V. COMPUTER SIMULATIONS

Computer simulations were executed to verify the derived masking region of the full array and subarray, i.e., (4), (5), (9), and (10). The DOA estimation performances of the proposed NFIM beamformer are compared with those of the conventional DAS and NFFF in [11].

A ULA utilized in the computer simulations consisted of 100 sensors with a 7.5 m sensor distance. Subarrays were configured with one sensor stride and 35 sensors satisfying (17). The sound speed was assumed as 1, 500 m/s. Multiple mixed near- and far-field sources were tested.

The conventional DAS outputs and the derived masking regions are shown for one near-field interferer in Fig. 4. Figs. 4(a) and (d) show the conventional DAS outputs when the near-field source was located at 450 m, and Figs. 4(b) and (e) demonstrate bearing time records (BTRs) when the near-field source approached 1, 500 m to 300 m. Figs. 4(c) and (f) show all subarray DAS outputs when the near-field source was located at 450 m. In Figs. 4(a), (b), and (c), the near-field source was located at 45°, and in Figs. 4(d), (e), and (f), the near-field source was located at 90°. The derived lower and upper masking azimuths are denoted as dashed lines and dashed-single dotted lines, respectively. In Fig. 4, the main beams of the near-field sources were well matched with the derived masking regions of the full array and subarrays.

In Figs. 5 and 6, the BTRs of the proposed beamformer and the conventional DAS for multiple mixed near- and far-field sources with mobilities are demonstrated. The simulation parameters are shown in Table 1, where the SNR denotes the signal-to-noise power ratio. The simulations were executed in two cases, i.e., single near-field interference and multiple near-field interferences. In Table 1, N1 and N2 denote the near-field interferences, and F1, F2, and F3 denote the far-field sources. All sources had the same sound pressure level (140 dB), and transmission loss was applied depending on the distance from the source to the sensor [17,18].

The BTRs of the conventional DAS and the proposed NFIM beamformer for one near-field interference are depicted in Fig. 5. In Fig. 5(a), the DOA estimations of F1 and F2, which were located in the masking region, were difficult, and only F3 at the outside of the masking region was detectable. However, Fig. 5(b) demonstrates that the proposed NFIM beamformer correctly detected all DOAs of three far-field sources.

In Fig. 6, the BTRs of the conventional DAS and the proposed beamformer for two near-field interferences are

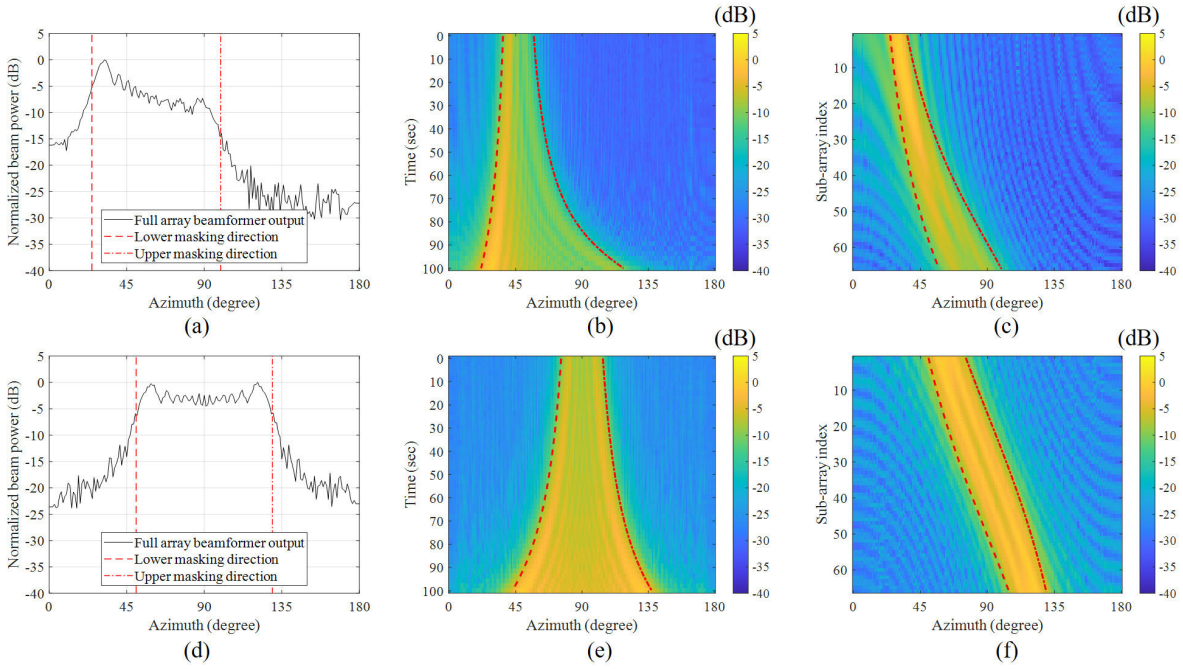

FIGURE 4. The derived masking regions: (a) and (d) the conventional DAS outputs of the full array at ($d_N = 450$ m, $\theta_N = 45°$) and ($d_N = 450$ m, $\theta_N = 90°$), respectively; (b) and (e) the BTRs of the full array at ($d_N = 300$ m-1500 m, $\theta_N = 45°$) and ($d_N = 300$ m-1500 m, $\theta_N = 90°$), respectively; (c) and (f) the conventional DAS outputs of all subarrays at ($d_N = 450$ m, $\theta_N = 45°$) and ($d_N = 450$ m, $\theta_N = 90°$), respectively.

TABLE 2. Simulation parameters for Figs. 5 and 6.

Figure	Source	Starting location			Ending location		
		azimuth	distance	SNR	azimuth	distance	SNR
Fig. 5	N1	80°	650 m	18 dB	95°	250 m	24 dB
	F1	70°	8, 250 m	1 dB	110°	8, 250 m	1 dB
	F2	100°	7, 500 m	2 dB	50°	8, 250 m	1 dB
	F3	140°	7, 500 m	2 dB	150°	7, 500 m	2 dB
Fig. 6	N1	60°	650 m	18 dB	60°	250 m	24 dB
	N2	110°	250 m	24 dB	110°	650 m	18 dB
	F1	60°	7, 500 m	2 dB	60°	7, 500 m	2 dB
	F2	120°	8250 m	1 dB	120°	8250 m	1 dB
	F3	150°	7, 500 m	2 dB	150°	8, 250 m	1 dB

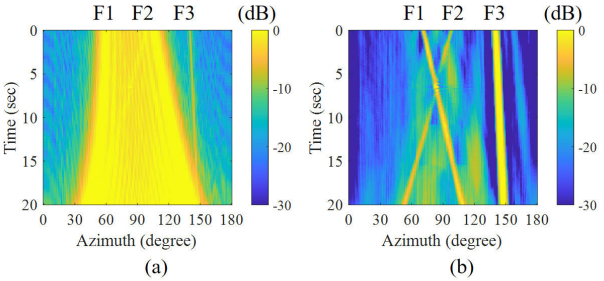

FIGURE 5. BTRs with a single near-field interference of (a) the conventional DAS beamformer and (b) the proposed NFIM beamformer.

depicted. In Fig. 6(a), F1 and F2 in the masking region were not detected, which is similar to Fig. 5(a). In Fig. 6(b), however, all of the far-field sources were detectable.

For the DOA estimation performance comparison of the proposed beamformer with the conventional DAS and the

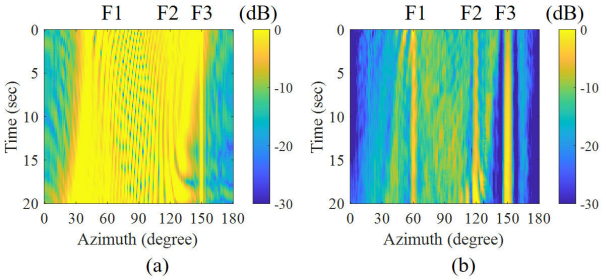

FIGURE 6. BTRs with multiple near-field interferences of (a) the conventional DAS beamformer and (b) the proposed NFIM beamformer.

NFFF, a peak-to-average power ratio (PAPR) and a root mean square error (RMSE) were utilized. The peak denotes the beam power at the DOA of the far-field source.

In Fig. 7, the PAPRs versus signal-to-interference power ratios (SIRs) of all methods were compared. In Figs. 7 (a) and (b), the interference-to-noise power ratios (INRs) were -10 dB and 10 dB, respectively. The azimuth of the near-field interference was 90°, and the distance was 450 m. The azimuth of the far-field source was the same as the near-field interference, and the distance was 7.5 km. Since the proposed method and the conventional NFFF methods utilized the estimated location information of the near-field interferences that have localization errors [19,20], localization errors were applied to the simulations. The distance estimation error varied from 0% to 5% with a uniform distribution, and the azimuth error varied from 0° to 1° with a uniform distribution. A solid black line denotes

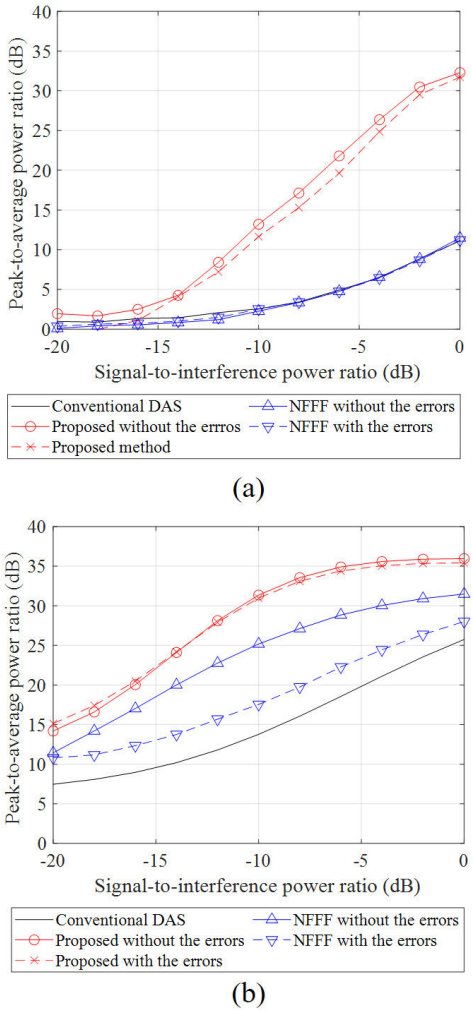

FIGURE 7. Comparison of the PAPRs versus SIRs of (a) INR = −10 dB and (b) INR = 10 dB.

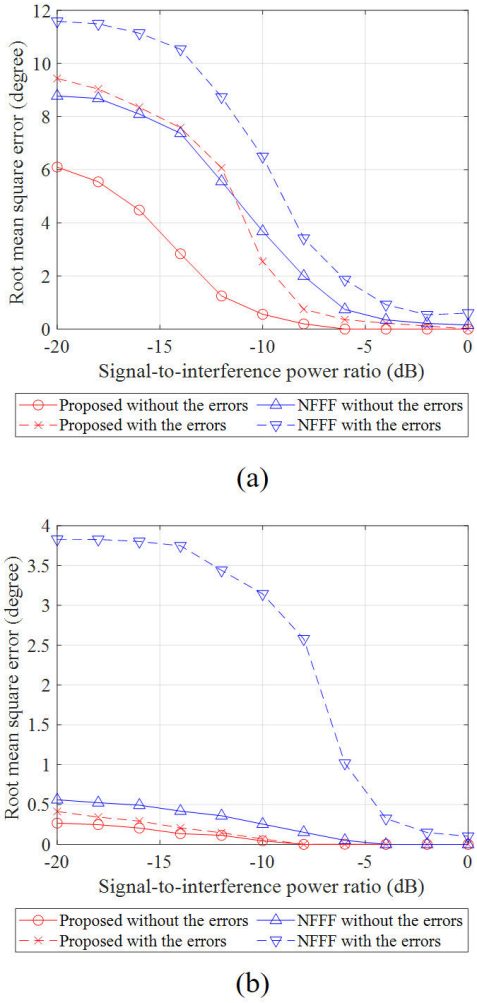

FIGURE 8. Comparison of the RMSEs versus SIRs of (a) INR = −10 dB and (b) INR = 10 dB.

the PAPR of the conventional DAS. An upper triangle and a lower triangle with a blue color denote that of NFFF without errors and with errors, respectively. A circle and an asterisk with a red color denote that of the proposed NFIM without errors and with errors, respectively.

In Fig. 7(a), the PAPR of the NFFF was similar to that of conventional DAS. At a PAPR of 10 dB, however, the proposed NFIM beamformer showed a 10 dB SIR gain compared to the conventional DAS and the NFFF. In Fig. 7(b), the PAPR of the conventional NFFF beamformer was degraded by the localization errors. However, the proposed NFIM demonstrated very small PAPR degradation due to localization errors. In Fig. 7(b), at a PAPR of 25 dB, the proposed NFIM method exhibited 4, 10, and 14 dB SIR gains compared to the conventional NFFF without errors, the conventional NFFF with errors, and the conventional DAS.

In Fig. 8, the RMSEs versus SIRs of the proposed NFIM beamformer and the conventional NFFF were compared. The simulation parameters were the same as in Fig. 7. In Fig. 8(a), even if no localization errors occurred, the RMSE of the NFFF did not converge to zero. However, when the SIR was equal to or greater than −6 dB, the RMSE of the proposed NFIM beamformer converged to zero. In Fig. 8(b), at a SIR of −10 dB, if localization errors occurred, the RMSE of the proposed NFIM beamformer increased by 0.02°, but that of the NFFF significantly increased by 2.89°. In Fig. 8(b), when the RMSE converged to zero, the proposed NFIM beamformer had a SIR of 4 dB gain compared to the conventional NFFF.

As shown in Figs. 7 and 8, the proposed NFIM beamformer demonstrated better DOA estimation performance than those of the conventional methods.

VI. CONCLUSION

This paper mathematically analyzed the masking region for a DOA estimator using a conventional DAS, and a subarray configuration for the beam separation of the far-field source from the near-field interference was derived. The interferences of all subarrays were suppressed by the proposed azimuth-domain filter. All outputs of the suppressed interferences for all subarrays were combined to mitigate the residual near-field interferences. Computer simulations demonstrated that the proposed NFIM beamformer had 4, 10, and 14 dB

SIR gains compared to the conventional NFFF without errors, the NFFF with errors, and the DAS, respectively, at a 25 dB of the PAPR. When the RMSE converged to zero, the proposed NFIM beamformer had a SIR of 4 dB gain compared to the conventional NFFF.

REFERENCES

[1] J. Li, Q. Lin, C. Kang, K. Wang, and X. T. Yang, "DOA estimation for underwater wideband weak targets based on coherent signal subspace and compressed sensing," *Sensors*, vol. 18, no. 3, pp. 1–19, Mar. 2018.
[2] Z. Ye, Y. Zhang, X. Xu, and C. Liu, "Direction of arrival estimation for uncorrelated and coherent signals with uniform linear array," *IET Radar, Sonar Navigat.*, vol. 3, no. 2, pp. 144–154, Apr. 2009.
[3] P. Palanisamy, N. Kalyanasundaram, and A. Raghunandan, "A new DOA estimation algorithm for wideband signals in the presence of unknown spatially correlated noise," *Signal Process.*, vol. 89, no. 10, pp. 1921–1931, Oct. 2009.
[4] N. N. D. Moura, J. M. Seixas, W. S. Filho, and A. V. Greco, "Independent component analysis for optimal passive sonar signal detection," in *Proc. 7th Int. Conf. Intell. Syst. Design Appl. (ISDA)*, Rio de Janeiro, Brazil, Oct. 2007, pp. 671–675.
[5] H.-J. Lee, J.-M. Ahn, J.-P. Seo, J.-K. Ahn, S.-I. Kim, and J.-H. Chung, "Left right discrimination performance improvement for the line array sonar system," *J. Acoust. Soc. Korea*, vol. 36, no. 1, pp. 49–56, Jan. 2017.
[6] H. Cox and H. Lai, "Sub-aperture beam-based adaptive beamforming for large dynamic arrays," in *Proc. Conf. Rec. 38th Asilomar Conf. Signals, Syst. Comput.*, Pracific Grove, CA, USA, Nov. 2004, pp. 2355–2358.
[7] M. Lasky, R. D. Doolittle, B. D. Simmons, and S. G. Lemon, "Recent progress in towed hydrophone array research," *IEEE J. Ocean. Eng.*, vol. 29, no. 2, pp. 374–387, Jul. 2004.
[8] A. Das, A. Kumar, and R. Bahl, "Marine vessel classification based on passive sonar data: The cepstrum-based approach," *IET Radar, Sonar Navigat.*, vol. 7, no. 1, pp. 87–93, Jan. 2013.
[9] L. Qiu, T. Lan, and Y. Wang, "A sparse perspective for direction-of-arrival estimation under strong near-field interference environment," *Sensors*, vol. 20, no. 1, pp. 1–21, Dec. 2019.
[10] G. Liang, W. Zhao, and Z. Fan, "Direction of arrival estimation under near-field interference using matrix filter," *J. Comput. Acoust.*, vol. 23, no. 4, pp. 1–13, Jan. 2016.
[11] L. Zhang, J. Mei, A. Zielinski, and P. Cai, "Direction-of-arrival estimation for far-field acoustic signal in presence of near-field interferences," *Electron. Lett.*, vol. 51, no. 1, pp. 101–103, Jan. 2015.
[12] M. Uthansakul and M. E. Bialkowski, "Wideband beam and null steering using a rectangular array of planar monopoles," *IEEE Microw. Wireless Compon. Lett.*, vol. 16, no. 3, pp. 116–118, Mar. 2006.
[13] Z. L. Yu, Z. Gu, J. Zhou, Y. Li, W. Ser, and M. H. Er, "A robust adaptive beamformer based on worst-case semi-definite programing," *IEEE Trans. Signal Process.*, vol. 58, no. 11, pp. 5914–5919, Jul. 2010.
[14] G. L. Liang, W. B. Zhao, J. Fu, and Z. Fan, "Adaptive beamforming algorithm with the near-field nulling weight," *J. Harbin Eng. Univ.*, vol. 36, no. 12, pp. 1549–1553, Dec. 2015.
[15] Y. Yang, Y. Zhang, and L. Yang, "Wideband sparse spatial spectrum estimation using matrix filter with nulling in a strong interference environment," *J. Acoust. Soc. Amer.*, vol. 143, no. 6, pp. 3891–3898, Jun. 2018.
[16] A. Hassanien, S. A. Elkader, A. B. Gershman, and K. M. Wong, "Convex optimization based beam-space preprocessing with improved robustness against out-of-sector sources," *IEEE Trans. Signal Process.*, vol. 54, no. 5, pp. 1587–1595, May 2006.
[17] J. M. Jornet, M. Stojanovic, and M. Zorzi, "On joint frequency and power allocation in a cross-layer protocol for underwater acoustic networks," *IEEE J. Ocean. Eng.*, vol. 35, no. 4, pp. 936–947, Oct. 2010.
[18] J. Khan and H.-S. Cho, "A distributed data-gathering protocol using AUV in underwater sensor networks," *Sensors*, vol. 15, no. 8, pp. 19331–19350, Aug. 2015.
[19] Z. Shang, W. Zhang, G. Zhang, X. Zhang, S. Ji, and R. Wang, "Mixed near field and far field sources localization algorithm based on MEMS vector hydrophone array," *Measurement*, vol. 155, no. 1, pp. 1–8, Feb. 2020.
[20] H. Liu, H. Meng, L. Gan, D. Li, Y. Zhou, and T. K. Truong, "Subspace and sparse reconstruction based near-field sources localization in uniform linear array," *Digit. Signal Process.*, vol. 106, no. 1, pp. 1–14, Aug. 2020.

HOJUN LEE was born in Pohang, South Korea, in 1990. He received the B.S. and M.S. degrees in electronics engineering from Inha University, Incheon, South Korea, in 2015 and 2018, respectively, where he is currently pursuing the Ph.D. degree in electronics engineering. His research interests include sonar systems, array signal processing, underwater acoustic communications, and machine learning.

JONGMIN AHN was born in Incheon, South Korea, in 1990. He received the B.S. and M.S. degrees in electronics engineering from Inha University, Incheon, in 2015 and 2017, respectively, where he is currently pursuing the Ph.D. degree in electronics engineering. His research interests include underwater acoustic communication, wireless communications, signal processing, and machine learning.

YONGCHEOL KIM was born in Jeju, South Korea, in 1995. He received the B.S. degree in electronics engineering from Inha University, Incheon, in 2018, where he is currently pursuing the Ph.D. degree in electronics engineering. His research interests include underwater acoustic communication systems, signal processing, estimation theory, and machine learning.

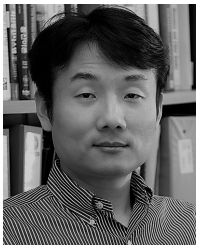

JAEHAK CHUNG received the B.S. and M.S. degrees from Yonsei University, Seoul, South Korea, in 1988 and 1990, respectively, both in electronics engineering, and the Ph.D. degree from The University of Texas at Austin, in 2000.

He is currently a Professor with Inha University, Incheon, South Korea. From 2001 to 2005, he was a Member of Technical Staff with the Samsung Advanced Institute of Technology (SAIT), Kyungkido, South Korea. His research interests include 6G, underwater acoustic communications, and machine learning.